Pattern formation on the surface of cationic-anionic cylindrical aggregates

Y. S. Velichko and M. Olvera de la Cruz*
Department of Material Science and Engineering, Northwestern University, Illinois 60208, USA
(Received 10 January 2005; published 19 October 2005)

Charged pattern formation on the surfaces of self-assembled cylindrical micelles formed from oppositely charged heterogeneous molecules such as cationic and anionic peptide amphiphiles is investigated. The net incompatibility χ among different components results in the formation of segregated domains, whose growth is inhibited by electrostatics. The transition to striped phases proceeds through an intermediate structure governed by fluctuations, followed by states with various lamellar orientations, which depend on cylinder radius R_c and χ. We analyze the specific heat, susceptibility $S(q^*)$, domain size $\Lambda=2\pi/q^*$, and morphology as a function of R_c and χ.

DOI: 10.1103/PhysRevE.72.041920 PACS number(s): 87.15.−v, 82.35.Pq, 81.16.Fg, 81.07.−b

Many heterogenous molecules, including lipids and amphiphiles, assemble into finite size aggregates or micelles [1–5]. Coassembly of cationic and anionic heterogeneous molecules is a route to create functional biomolecular materials, such as stable vesicles for drug delivery [1,2] and bioactive fibers [3,4]. Coassembled cationic and anionic systems are ubiquitous in nature since most biomolecules are heterogenous, charged and strongly associating in aqueous solutions. The competition of long-range electrostatic and short-range interactions among different coassembled components may lead to the formation of complex aggregates with surface charge heterogeneities. These heterogeneities are expected to play a prominent role in the fabrication of functional assemblies and in the self-organization of the aggregates.

The assembly of single component charged amphiphilic molecules is restricted by electrostatic repulsion [6,7]. For example, electrostatics restricts assembly of charged peptide amphiphiles (PA) composed of a hydrophobic block connected to a peptide block that favors β-sheet formation. Single component PAs assemble only when the peptide blocks are neutral (acidic PAs assemble at high pH and basic PAs at low pH conditions) and/or when the salt concentration is excessively high. However, at physiological pH conditions, when the molecules are charged, stoichiometric mixtures of acidic (−) and basic (+) PAs coassemble at one percent concentration into nanofibers of diameter about 6–8 nm and a few microns length, which form a network that resembles extracellular matrix found in living tissue [3]. The peptide amphiphile charged end groups are exposed to the surface of the fibers, and their amino acids sequences can be designed to promote the growth of bone [8], or neural cell differentiation [4].

Coassembled neutral molecules, such as phospholipids and cholesterol in mono or bi-layers, are generally unstable. These neutral assemblies generate domains of different density or composition along the surface, which coarsen with time [5] and, eventually, lead to the dissolution of the coassembled structure [9]. Instead, in coassembled chemically dissimilar cationic and anionic amphiphile mixtures, the compositional heterogeneities driven by a net incompatibility among the different components are stabilized by electrostatics, which favors mixing of the charged components. At low temperature T, the competition of the interfacial energy (which favors large domains) and the electrostatic interactions (which favors small domains) is expected to result in periodic surface charged domains [10,11] of size Λ. In this letter we study the formation of charged domains in cylindrical aggregates with Coulomb interactions at various degrees of incompatibility and cylinder radii. We analyze charge correlations and domain orientations, as well as the thermodynamics of the local segregation process. We show that phase segregation on the surface of coassembled cationic-anionic micelles can be readily observed when the net incompatibility among dissimilar molecules generated by chemical and/or molecular sizes differences is larger than a couple k_BT's.

We consider each aggregate as a stable structure, thus constraining the cylindrical geometry of the micelles and examining only equilibrium surface structures. A binary electroneutral charged lattice fluid consisting of positive and negative units of equal absolute charge $|Q_+|=|Q_-|$, confined to a cylindrical monolayer of radius R_c and length $L_c=L_z$, is placed in the center of the box $L\times L\times L_z$ along the z axis. The surface of the cylinder is filled with spherical units of diameter $\sigma=1$, in such a way, that all units are placed into the knots of a triangular lattice of period $a=\sigma$ (Fig. 1). The net degree of compatibility in k_BT units ($\chi=n[\varepsilon_{+-}-(\varepsilon_{--}+\varepsilon_{++})/2]$, where $n=6$ is the number of nearest neighbors) in our incompressible model is simply $\chi=-3\varepsilon_{++}$, because for simplicity we only consider short-range nonelectrostatic attraction among positively charged molecules (in a compressible model all the interactions have to be included). It should be noted here that χ describes the effective non–electrostatic interaction among the coassembled macromolecules and not among single monomers. In the systems with only van der Waals interactions χ is proportional to $1/T$, however, systems with hydrophobic and hydrogen bonding interactions, such as in coassembled PA's, the pair interaction may have a complex T dependence. Excluded volume and electrostatic interactions are also considered. The Hamiltonian of the system reads as follows:

*Electronic address: m-olvera@northwestern.edu

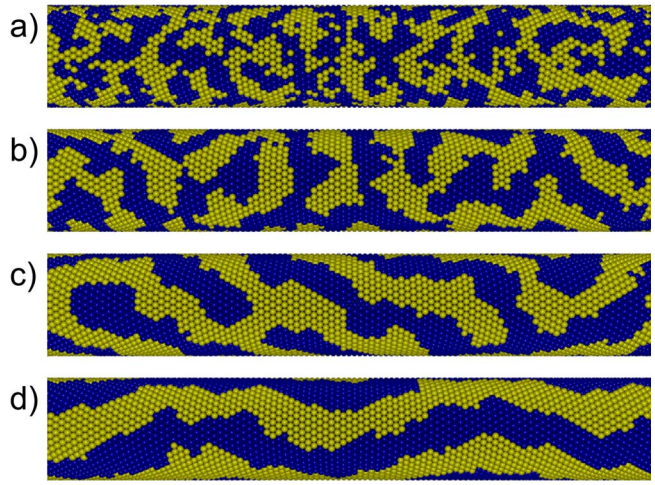

FIG. 1. (Color online) Snapshots of typical configurations of (a) isotropic phase (χ=4.5), (b) locally correlated state (χ=6.75), (c) striped state with defects (χ=9.0), and (d) parallel striped phase (χ=12.0). R_c/σ=8.

$$\frac{H}{k_BT} = \sum_{i>j}^{N} \frac{Q_iQ_j}{\epsilon_o r_{ij}} + \sum_{\{i,j\}}^{N} \frac{\varepsilon_{++}(Q_i+Q_+)(Q_j+Q_+)}{(2Q_+)^2}, \qquad (1)$$

where Q_i is a charge of the ith unit, ϵ_o is the average dielectric constant of the media in units $e^2/4\pi\sigma$, $r_{ij}=|\vec{r}_j-\vec{r}_i|/\sigma$ is a dimensionless distance between ith and jth units, $\vec{r}_i$ determines the position of the ith unit in the space, $Q_+=1$ and the summation in the second term is only over nearest neighbors. To exclude interaction with displaced image–cylinders, periodical boundary conditions are applied only in the z direction and, thus, Lekner summation technique [12] is used to calculate the electrostatic energy of the single cylinder system

$$\frac{E_{el}}{k_BT} = \frac{1}{2\epsilon_o} \sum_{i,j=0}^{N} \sum_{m=-\infty}^{\infty} \frac{Q_iQ_j}{\sqrt{\rho_{ij}^2+(z_{ij}+mL_z)^2}}, \qquad (2)$$

where $\rho_{ij}=[x_{ij}^2+y_{ij}^2]^{1/2}$ and for $m=0$ the terms with $i=j$ are omitted. We report standard canonical Monte Carlo simulations following the Metropolis scheme for various values of $\varepsilon_{++}\in[-4.5,-0.5]$, $\epsilon_o=10$, $R_c/\sigma\in[1,8]$ and $L_c/\sigma=100$. Simple moves in the phase space are performed by exchange of two randomly chosen particles. Each system is equilibrated during 10^5 MC steps per particle and another 10^5MC steps are used to perform measurements. The equilibration process is accompanied by a gradual decrease of temperature (temperature annealing) from $T_{max}=10$ to $T_{min}=1$. To analyze equilibrium properties we calculate the heat capacity C_V and the static structure factor

$$S(q) = \frac{1}{N_+}\left\langle \left| \sum_{i,j=0}^{N_+} e^{i\vec{q}\cdot(\vec{s}_j-\vec{s}_i)} \right|^2 \right\rangle, \qquad (3)$$

where $\vec{s}_j$ is a two-dimensional Cartesian surface vector and $S(q)$ is averaged among different directions. We focus our attention on the size of the segregated domains and on the susceptibility, a degree of correlations in the system.

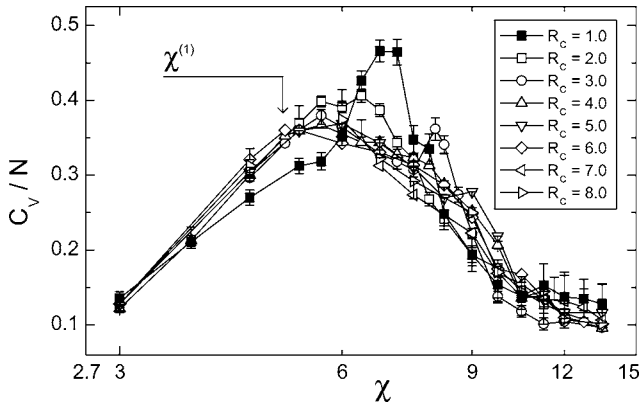

FIG. 2. Dimensionless, normalized by N, heat capacity as a function of the pair attraction energy χ for different R_c.

The transition from the isotropic to the striped phase begins with the appearance of segregated domains [Fig. 1(a)] and proceeds through an intermediate locally correlated state governed by fluctuations [Fig. 1(b)]. In the planar (2D-monolayer) case, in the limit of zero charge, a macroscopic phase segregation in the mean field approximation is expected at a critical point $\chi^{cp}\simeq 2$, as predicted by a simple coarse-grained free energy functional of the neutral system [13],

$$\frac{\Delta F(\phi)}{k_BT} = \int \frac{f(\phi)+\kappa|\nabla\phi|^2}{\sigma^2} d^2r, \qquad (4)$$

where $\phi=\phi(\mathbf{r})$ is the local charge concentration, $f(\phi)=\phi\ln\phi+(1-\phi)\ln(1-\phi)-\chi\phi^2$, $\kappa\approx\chi a^2/2$ [14]. In the charged case there is no critical point. Instead, a broad peak in the heat capacity (Fig. 2) at a characteristic value denoted by $\chi^{(1)}$ is observed. The charges restricts the possibility of macroscopic segregation and induces instead favorable fluctuations of wave length λ. If the charge fluctuations are small, a density variation till second order in the free energy in terms of the Fourier components of the density ϕ_q gives $\Delta F/k_BT\sim\Sigma_q\phi_q\phi_{-q}/(2S_0(q))$, where $S_0^{-1}(q)=4-2\chi+\chi q^2+8\pi/q\epsilon_o$. The competition between electrostatic, $8\pi/q\epsilon_o$, and gradient, χq^2, energies results in the formation of most favorable fluctuations of finite wave length $\lambda=2\pi/q^*$ and the appearance of a peak in $S_0(q)$ at $q^*=(4\pi/\epsilon_o\chi)^{1/3}$ as shown in the computed $S(q)$ in Fig. 3(a). This scaling regime is possible for $\chi<\chi^{(1)}$ (fluctuations are expected to modify this mean field scaling) [Fig. 3(c)]. On the other hand, in the high χ limit (low T), strongly segregated charged domains of size Λ with a well defined line tension $\gamma\sim\chi$ [15] develop. The competition of the interfacial energy among the segregated domains, $\gamma\Lambda$, and the electrostatic penalty associated with creating a charge domain, $(\Lambda^2)^2/(\epsilon_o\Lambda)$, gives another scaling limit $\Lambda\sim(\epsilon_o\chi)^{1/2}$ [10]. The second scaling regime is found to exist for $\chi>\chi^{(2)}$, where $\chi^{(2)}$ is defined below.

The mean-field analysis of Eq. (4) erroneously predicts a continuous transition to a periodic structure signaled by a mean field susceptibility $S_0(q^*)=\infty$ at $\chi_{cp}=2+(3/2)\times[4\pi\sqrt{\chi_{cp}}/\epsilon_o]^{2/3}$. It is well known that the transitions from isotropic to periodic structures cannot be continuous [16]. In

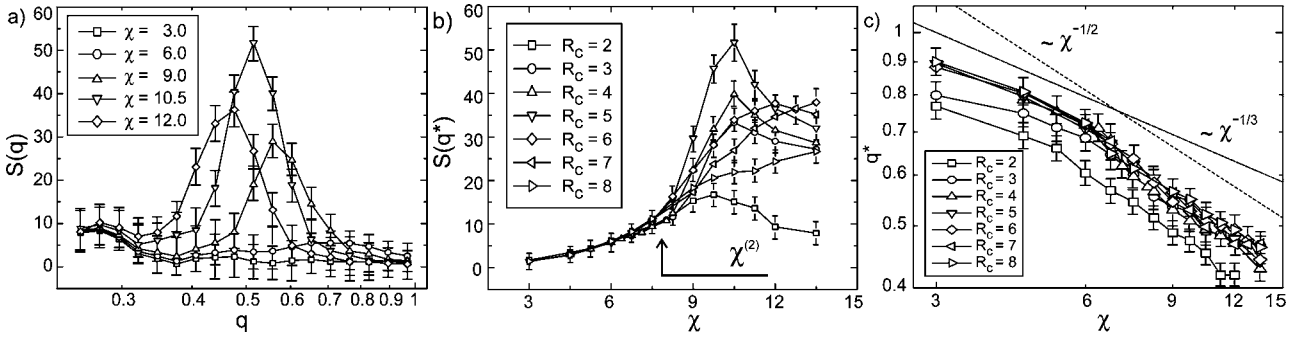

FIG. 3. (a) Static structure factor for $R_c=5$ for different χ, (b) magnitude of the peak of the structure factor, $S(q^*)$, as a function of χ for different R_c values, and (c) double logarithmic plot of the peak position q^* versus χ for different R_c.

3D the electrostatically driven microphase separation [17] is often suppressed by various effects [18]. Since long-range order in 2D systems with $1/r$ interactions is uncertain [19,20], the possibility of a classical thermodynamic transition to periodic structures is questionable. In 1D, on the other hand, fluctuations destroy the possibility of either macro–phase or microphase transitions at nonzero T [21]. We expect to recover the 2D limit only when $R_c\to\infty$ and the 1D case when $R_c\to 0$.

Appearance of large domains on the surface of the cylinder of final radius applies geometrical restrictions on the size and symmetry of the domains, especially in the 1D–limit. These geometrical restrictions may influence physical properties, such as the susceptibility. Figure 3(b) shows a nonmonotonic dependence of $S(q^*)$ with χ. We find that $S(q^*)$ is independent of R_c for $\chi<\chi^{(2)}$, while for $\chi>\chi^{(2)}$ it shows a non monotonic dependence on R_c. The point $\chi^{(2)}$ corresponds to the crossover transition from the state, where the segregated domains are locally correlated, to the striped state, where the domain size scales as $\Lambda\sim(\epsilon_o\chi)^{1/2}$ and the domains morphology depends on R_c. The melting of striped structures in the limit $R_c\to\infty$ may occur via the Kosterlitz-Thouless mechanism [22]. Besides the appearance of dislocations and other defects (Fig. 1(c)), the striped state on the cylinder is richer due to the possibility of different symmetries. We find a broad peak in $S(q^*)$ versus R_c [Fig. 4(a)] for each $\chi>\chi^{(2)}$, implicitly denoted by $\chi^{(3)}$, that moves to larger R_c values with increasing χ. For intermediate $\chi>\chi^{(2)}$ the structures are strongly dependent on R_c. For very wide cylinders ($q^*R_c>2.5$) we find a defect mediated striped state. With decreasing R_c the striped state turns into the spiral/zigzag state ($1<q^*R_c<2.5$). With further decreasing R_c the spiral/zigzag phase, first, turns into a parallel lamella and then into the ring phase ($q^*R_c<1$). With increasing the energy χ, the spiral state turns into the zigzag state and then into the parallel striped phase. Our simulation shows that for large χ the parallel stripe phase dominates unless the $q^*R_c\sim 1$.

We calculate an order parameter with the purpose of characterizing the geometry of the domains and to find their preferable morphology. We begin by defining independent clusters on the surface of the cylinder. For each cluster $\mathcal{C}$ we calculate the inertia matrix with components

$$T_{\alpha\beta}=\frac{1}{N_{\mathcal{C}}^2}\sum_{i>j}^{N_{\mathcal{C}}}(r_i^\alpha-r_i^\beta)(r_j^\alpha-r_j^\beta), \tag{5}$$

where $N_{\mathcal{C}}$ is the number of ions in the $\mathcal{C}$ cluster and r_i^α is the αth Cartesian component of the position vector of the ith ion. To characterize the anisotropy of the cluster we use the "asphericity parameter" introduced by Rudnick and Gaspar [23]

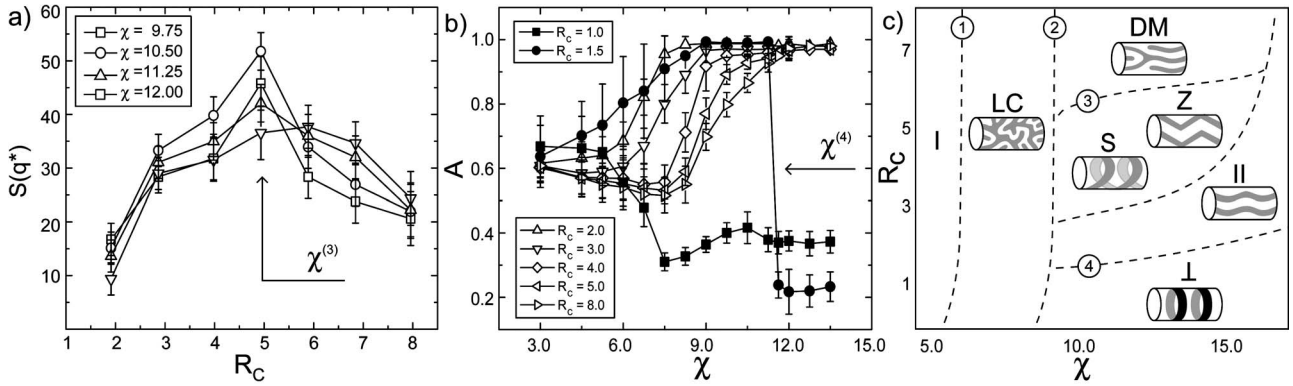

FIG. 4. (a) Susceptibility $S(q^*)$ as a function of R_c near extremum, (b) asphericity order parameter as a function of χ and R_c, (c) schematic phase diagram (χ,R_c) implied by results of simulation, where I is the isotropic phase, II is the parallel lamella phase, $\perp$ is the ring phase, LC is the locally correlated state, S is the helically twisted state, Z is the zigzag state, and DM is the defect mediated state. Lines (1), (2), (3), and (4) correspond to $\chi^{(1)}$, $\chi^{(2)}$, $\chi^{(3)}$, and $\chi^{(4)}$.

$$A = \frac{\langle (\mathrm{Tr}[T])^2 - 3M[T] \rangle}{\langle (\mathrm{Tr}[T])^2 \rangle}, \tag{6}$$

where (R_1^2, R_2^2, R_3^2) are the eigenvalues of the matrix $T_{\alpha\beta}$ which defining the three principal axes of the cluster, $\mathrm{Tr}[T]=R_1^2+R_2^2+R_3^2$ is the trace, $M[T]=R_1^2R_2^2+R_1^2R_3^2+R_2^2R_3^2$ is the sum of three minors and A is averaged among all clusters. For spherically symmetric objects $(R_1=R_2=R_3)$ A is equal to zero, for thin toroidal objects $(R_1=R_2, R_3 \ll R_1)$ it is equal to $A \simeq 1/4$ (in our case, ring phase) and for long thin stripes $(R_2 \ll R_1, R_3 \ll R_1)$ $A \simeq 1$ (parallel lamella phase). Figure 4(b) shows A as a function of χ. For small values of χ, when system is isotropic, the asphericity parameter takes value $A \simeq 0.6$ independent on R_c. For wide cylinders $(q^* R_c > 1)$ A grows with χ and approaches unity at large χ values. For relatively thin cylinders, $q^* R_c \simeq 1.5$, it approaches unity faster than for cylinders with $q^* R_c \simeq 2.5$, due to the fact that A does not distinguish stripes in parallel, spiral or zigzag states. Meanwhile, for the stripes disturbed by the defects $(q^* R_c \geqslant 2.5)$ the asphericity parameter takes smaller values than unity. In the case of thin cylinders $(q^* R_c < 1)$ the asphericity parameter A indicates formation of ring stripes. The transition from the parallel lamellar phase to the ring phase is found at χ denoted by $\chi^{(4)}$.

Our results are summarized in Fig. 4(c), where we show a schematic (χ, R_c) phase diagram. We predict various micro–phases obtained as a result of the interplay of short- and long–range forces among stoichiometric charged components confined on the surface of a cylindrical fiber. Our study suggests that besides modifying the size and the chemistry of the molecules to induce different domain symmetries, one can coassemble basic and acidic molecules with different total charge per molecule, e.g., +2 and −1, which may induce other domain symmetries along the surface of the cylinder [10]. Various different symmetries and interesting phenomena appear as a result of the interplay between the symmetry of the surface domains and the geometry of the aggregates. The constraint of tiling the surface of aggregates with finite size domains of different symmetries is a topic of interest and is relevant to studies of viral symmetry and other self-assembled supramolecular structures.

We acknowledge valuable discussions with S. I. Stupp, F. J. Solis, and A. Kudlay. This work is supported by NSF grant numbers DMR-0414446 and DMR-0076097, and by NIH grant number GM62109.

[1] M. Dubois, B. Deme, T. Gulik-Krzywicki, J. C. Debieu, C. Vautrin, E. Perez, and T. Zemb, Nature (London) **411**, 672 (2001).
[2] E. W. Kaler, K. L. Herrington, A. K. Murthy, and J. A. N. Zasadzinski, J. Phys. Chem. **96**, 6698 (1992).
[3] K. L. Niece, J. D. Hartgerink, J. J. J. M. Donners, and S. I. Stupp, J. Am. Ceram. Soc. **125**, 7146 (2003).
[4] G. A. Silva, C. Czeisler, K. L. Niece, E. Beniash, D. A. Harrington, J. A. Kessler, and S. I. Stupp, Science **303**, 1352 (2004).
[5] S. L. Veatch and S. L. Keller, Phys. Rev. Lett. **89**, 268101 (2002).
[6] C. Huang, M. Olvera de la Cruz, M. Delsanti, and P. Guenoun, Macromolecules **30**, 8019 (1997).
[7] O. V. Borisov and E. B. Zhulina, Macromolecules **36**, 10029 (2003).
[8] J. D. Hartgerink, E. Beniash, and S. I. Stupp, Science **294**, 1684 (2001).
[9] M. Laradji and P. B. Sunil Kumar, Phys. Rev. Lett. **93**, 198105 (2004).
[10] F. J. Solis, S. I. Stupp, and M. Olvera de la Cruz, J. Chem. Phys. **122**, 054905 (2005).
[11] R. P. Feynman, R. B. Leighton, and M. Sands, *The Feynman Lectures in Physics* (Addison-Wesley, Reading, MA, 1964), Sec. II.8.3.
[12] A. Grzybowski, and A. Bródka, Mol. Phys. **100**, 635 (2002).
[13] J. W. Cahn and J. E. Hilliard, J. Chem. Phys. **28**, 258 (1958).
[14] For exact values in 2D Ising model, see T. T. Wu, B. M. McCoy, C. A. Tracy, and E. Barouch, Phys. Rev. B **13**, 316 (1976).
[15] P. M. Chaikin and T. C. Lubensky, *Principle of Condensed Matter Physics* (Cambridge University Press, Cambridge, UK, 1995).
[16] S. A. Brazovskii, Sov. Phys. JETP **41**, 85 (1975).
[17] E. E. Dormidontova, I. Y. Erukhimovich, and A. R. Khokhlov, Macromol. Theory Simul. **3**, 661 (1994).
[18] R. Chang and A. Yethiraj, J. Chem. Phys. **118**, 6634 (2003).
[19] N. D. Mermin, Phys. Rev. **176**, 250 (1968).
[20] M. Baus, J. Stat. Phys. **22**, 111 (1980).
[21] A. Ben-Naim, *Statistical Thermodinamics for Chemists and Biochemists* (Plenum Press, New York, 1992).
[22] D. R. Nelson, *Defects and Geometry in Condensed Matter* (Cambridge University Press, Cambridge, UK, 2002).
[23] J. Rudnick, and G. Gaspari, J. Phys. A **19**, L191 (1986).